

REPORT DOCUMENTATION PAGE

Form Approved

OMB No 0706-0188

Public reporting burden for this collection of information is estimated to average 1 hour per response, including the time for reviewing instructions, searching existing data sources, gathering and maintaining the data needed, and completing and reviewing the collection of information. Send comments regarding this burden estimate or any other aspect of this collection of information, including suggestions for reducing this burden, to Washington Headquarters Services, Directorate for Information Operations and Reports, 1215 Jefferson Davis Highway, Suite 1204 Arlington, VA 22202-4302 and to the Office of Management and Budget, Paperwork Reduction Project (0706-0188) Washington, DC 20503.

1. AGENCY USE ONLY (Leave blank)		2. REPORT DATE <i>Dec</i> February 1997	3. REPORT TYPE AND DATES COVERED Final Report (09/01/95-08/31/97)
4. TITLE AND SUBTITLE Characterization of Mechanical Properties of Interphase in Glass/Polyester Composite System			5. FUNDING NUMBERS DAAH04-95-1-0543
6. AUTHOR(S) Fu-Pen Chiang Principal Investigator			8. PERFORMING ORGANIZATION REPORT NUMBER
7. PERFORMING ORGANIZATION NAME(S) AND ADDRESS(ES) Dept. of Mechanical Engineering State University of New York at Stony Brook Stony Brook, NY 11794-2300			10. SPONSORING MONITORING AGENCY REPORT NUMBER ARO 34927.1-MS
9. SPONSORING/MONITORING AGENCY NAME(S) AND ADDRESS(ES) U.S. Army Research Office P. O. Box 12211 Research Triangle Park, NC 27709-2211			11. SUPPLEMENTARY NOTES The views, opinions and/or findings contained in this report are those of the author(s) and should not be construed as an official Department of the Army position, policy, or decision, unless so designated by other documentation.
12a. DISTRIBUTION/AVAILABILITY STATEMENT Approved for public release; distribution unlimited.			12b. DISTRIBUTION CODE
13. ABSTRACT (Maximum 200 words) A bimaterial pair consisting of homopolymers PMMA (polymethylmethacrylate) and PS (polystyrene) was selected for this study. A graft copolymer was used to bind the two homopolymers together. Instead of the conventional asymmetric double cantilever beam test we selected the asymmetric four-point-bend test scheme to evaluate the bimaterial system, because the latter can be employed to evaluate the effect of mode mixity. The mechanical properties of PMMA and PS are quite similar; thus the resulting Dunder's parameters are very small. Yet the material pair exhibits strong characteristics of a typical bimaterial. As it turned out the two materials have distinctly different fracture mechanisms. PMMA fails by generating a large amount of microcrack whereas PS fails by crazing which consumes much more energy. Depending upon the mode mixity an interfacial crack can be driven either into PMMA or into PS. And the resulting fracture toughnesses are quite different. Detailed strain distributions at the crack tips were mapped by the micromechanics technique called SIEM (Speckle Interferometry with Electron Microscopy) which provides the foundation for the fracture mechanism.			
14. SUBJECT TERMS			15. NUMBER OF PAGES
			16. PRICE CODE
17. SECURITY CLASSIFICATION OF REPORT UNCLASSIFIED	18. SECURITY CLASSIFICATION OF THIS PAGE UNCLASSIFIED	19. SECURITY CLASSIFICATION OF ABSTRACT UNCLASSIFIED	20. LIMITATION OF ABSTRACT UL

**Final Report
To
Army Research Office**

**P. O. Box 12211
4300 South Maimi Boulevard
Research Triangle Park
North Carolina 27709-2211**

**on Grant No. DAAH049510543
(Dr. Rober R. Reeber, Program Director)**

**“Characterization of Mechanical Properties of
Interphase in Glass/Polyester Composite System”**

by

**Fu-Pen Chiang
Department of Mechanical Engineering
State University of New York at Stony Brook
Stony Brook, NY 11794-2300**

DTIC QUALITY INSPECTED 2

December 1997

19980519 027

Table of Content

1. Introduction	2
2. Tailoring Interphase Strength	3
3. PS/PMMA Material Pair Selected for Study	4
4. Evaluation of Adhesion by Asymmetric Double Cantilever Beam Test	5
5. Experimental Macro- and Micro-mechanics Study by Using Asymmetric Four Point Bend Test and SIEM	7
6. Fracture Mechanism at PS/PMMA Interfacial Crack Tip	9
7. PS/PMMA Interfacial Crack Tip Field	12
8. References	13
9. Publications/Presentations Resulting from This Support	15
10. Personnel Participated in This Project	15
11. Figures	16

1. Introduction:

Composite materials such as polymer alloys or blends can be tailored to exhibit a desired optical, electrical, mechanical, or rheological properties for a variety of specific applications. However, actual fabrication of such composites poses significant challenges, one of which is the design and control of adhesion between different constituents. The adhesion of polymer interface can vary from very strong to extremely weak. The structural integrity and mechanical properties of the resulting composite material are largely dependent on the strength of the interphase (the thin layer of material that exists at the interface) that connects two neighboring constituent materials. To meet different requirements in various applications, recent research activities have been focusing more on the development of polymer systems with controlled interface properties than the optimization of bulk properties.

This research project is an attempt to answer some questions related to this challenge of interphase design, fabrication and characterization. Some of the questions that need to be asked are: (1) What is the precise role that an interphase plays in controlling the toughness of a composite material? (2) Which microstructural parameter governs the interphasial fracture behavior? (3) How can one use mechanistic principles to guide the design of a composite material?

2. Tailoring Interphase Strength:

To design and predict the mechanical behavior of a composite, it is necessary to have the interphase strength varied in a controlled manner. The first efforts of this research is to find an efficient way to form an interfacial bond between polymer glass and polyester and to quantify the characteristics of the bond. Different homopolymers are normally not miscible due to their inherent thermodynamic incompatibility, because the large size of the macromolecules ensures that there is very little mixing entropy available. As a result, the equilibrium state attained at the interface between two immiscible polymers gives rise to an extremely thin “interphase” whose thickness is only of the order of nanometers.^[1,2] Chains within the interphase region do not normally interpenetrate significantly; hence the adhesion strength of a polymer-polymer interphase is intrinsically low.

There are a few techniques which can be applied to modifying the polymer-polymer interphase structure. By decreasing the interfacial tension and increasing the interpenetration and entanglement of molecules, these techniques can enhanced the adhesive properties considerably. One of the most studied technique is the addition of an A-B block copolymer between A and B homopolymers. If the block copolymer is correctly designed such that each of its blocks is miscible with one or the other of the homopolymers, it will localize at the polymer-polymer interface resulting in the A-block

interpenetrating into the A-homopolymer chains and the B-block interpenetrating into the B-homopolymer chains as schematically shown in Fig.1. A small amount of such a copolymer can markedly enhances the strength of adhesion.^[3-7]

3. PS/PMMA Material Pair Selected for Study

The homopolymers PS(polystyrene) and PMMA(polymethylmethacrylate) of commercial grade purchased from Aldrich Chemical Company were chosen as the material system for this study. Their bulk properties are listed in table I. The coupling agent for the system is a PMMA-g-PS graft copolymer with a PMMA backbone of 120,000 and three PS chains of 40,000. Its architecture is schematically shown in Fig.2.

Table I: Properties of bulk polymers

	MW	E (MPa)	ν	T_g (°C)
PS (1)	280,000	3000	0.341	100
PMMA (2)	120,000	3300	0.325	105

MW: Average Molecular Weight,

E: Young's Modulus,

ν : Poisson Ratio,

T_g : Glass-Transition Temperature.

To prepare the specimen, sheets of PS and PMMA were first compression molded at 320°F and 300°F, respectively. The PS-PMMA graft copolymer, dissolved in appropriate solvents, was spun cast onto the PMMA sheet. To quantify the amount of copolymer, a copolymer film was spun on a silicon wafer. By an ellipsometry technique, the film thickness was measured with an accuracy of ± 3 Å. With the same solution concentration and spin speed, the copolymer was cast onto the surface of a PMMA sheet. The PMMA sheets were then placed into a vacuum oven at 80°C to expel the residue solvent. After that, the sandwich of PS, PS-g-PMMA and PMMA was heated to the joining temperature of 300°F under slight pressure and annealed for 60 minutes. The samples were allowed to cool in the mold for 2 to 3 hours until reaching the room temperature in an effort to minimize the formation of thermal stress. To create an interfacial crack, a piece of Teflon tape was used to cover part of the interface region on the PS side before the PS and PMMA sheets were joined together.

4. Evaluation of Adhesion Strength by the Asymmetric Double Cantilever Beam (ADCB) Test:

The concept of fracture toughness has been widely used as a means to evaluate the interface adhesion. The most commonly adopted test specimen is the asymmetric double cantilever beam (ADCB) (see Fig.3), whereby the interfacial fracture toughness G_c can be obtained with the assumption that upon fracture all the elastic energy is dissipated in a very small region ahead of the crack tip. This model assumes that the released elastic energy comes only from the bending of the two beams. Under this condition, G_c is given by^[8]

$$G_c = \frac{3u^2 E_1 D_1^3 E_2 D_2^3}{8a^4 [E_1 D_1^3 + E_2 D_2^3]} \quad (1)$$

where u is the wedge thickness; E_1 and E_2 are the Young's moduli of the materials; D_1 and D_2 are the thicknesses of the two layers; and a is the crack length. This approximation is valid only when the crack length is very large compared to the sample thickness, which is the case for a weak interface. When the sample is attached to a rigid substrate as shown in Fig.4, it can be modeled as a single cantilever beam on an elastic foundation and the expression for the G_c reduces to^[8]

$$G = \frac{3ED^3 u^2}{8a^4 [1 + (0.64D/a)]^4} \quad (2)$$

where a is the crack length, u the thickness of wedge, D the beam depth and E the Young's modulus.

ADCB test is performed by inserting a wedge (usually a single-edged razor blade) at the interface and pushing it in at a very slow speed. From the measurement of the razor

blade thickness and crack length ahead of the blade, fracture toughness can be obtained from Eq.(2). From ADCB tests, it is found that PS/PMMA copolymer improves the fracture toughness of the interface between PS and PMMA by more than one order of magnitude as shown in Fig.5. The term “interface thickness” in the figure does not describe the physical dimension of an interphase. It is a measure of the amount of the copolymer added onto the interface. In other words, the interfacial bonding condition is quantified and controlled by the amount of copolymer.

The ADCB test is convenient and effective. But it is an approximation. Moreover, the calculated value of critical energy release rate is inversely proportional to the measured crack length to the fourth power. Small error of the measurement can cause large data scattering. More importantly, it does not reveal the mode mixity behavior of a bimaterial interfacial fracture. In order to overcome these drawbacks, we have adopted the asymmetric four-point bend test and the results are presented in the following section.

5. Experimental Macro- and Micro-mechanics Study by Using Asymmetric-Four-Point-Bend Test and SIEM:^[12,13]

The asymmetric four-point-bend specimen, as schematically shown in Fig.6, has been calibrated by O'Dowd, Shih and Stout^[9]. This asymmetric bend crack geometry together with the symmetric geometry can provide interface toughness data for the full range of

mode mixities between mode I and mode II. The complex stress intensity factor can be expressed in the generic form of:

$$K = YT\sqrt{L}L^{-i\epsilon}e^{i\psi} \quad (3)$$

where L is a characteristic dimension of the crack geometry which is taken as the crack length here. T is a representative stress amplitude. Y is a dimensionless geometric factor and ψ is the phase angle of the tractions at the distance L from crack tip:

$$T = \frac{P}{W} \left[\frac{B-A}{B+A} \right], \quad Y = \sqrt{Y_1^2 + Y_2^2}, \quad \psi = \tan^{-1} \left\{ \frac{Y_2}{Y_1} \right\} \quad (4)$$

where A, B, W are geometric parameters of the test beam and

$$\text{for positive phase angles:} \quad Y_1 = (6s/W)f_1 - 2\epsilon g_1 \quad (5)$$

$$Y_2 = f_2 + (12s/W)\epsilon g_2 \quad (6)$$

$$\text{and for negative phase angles:} \quad Y_1 = (6s/W)f_1 + 2\epsilon g_1 \quad (7)$$

$$Y_2 = -f_2 + (12s/W)\epsilon g_2 \quad (8)$$

where f_1, f_2, g_1, g_2 are calibration functions. The energy release rate is given by

$$G = \frac{1 - \beta^2}{E^*} |K|^2 \quad (9)$$

The effective modulus E^* is defined by

$$\frac{1}{E^*} = \frac{1}{2} \left(\frac{1}{E_1'} + \frac{1}{E_2'} \right) \quad \text{and} \quad \frac{1}{E'} = \frac{E}{1 - \nu^2} \quad \text{for plane strain.} \quad (10)$$

In addition to fracture toughness, we have performed micromechanics studies of the crack tip field. For measuring deformation we employed the technique SIEM(speckle

interferometry with electron microscopy) which is an experimental micromechanics technique recently developed by the principal investigator.^[10,11] It has a displacement resolution of a few nanometers and is capable of mapping deformation within a region of only a few microns. By using the SIEM technique, the strain field at the interfacial crack tip was determined. In order to relate the microscopic mechanism to the macroscopic overall behavior, a special test fixture was designed and built such that it is suitable not only for measuring macroscopic properties, such as fracture toughness, using an ordinary testing machine, but also for determining the micromechanical response of the interface employing an environmental scanning electron microscope (SEM). In addition, fracture tests performed inside the environmental SEM allowed an in situ observation of the failure process of polymers without metallic coating. Results are presented in the following two sections.

6. Fracture Mechanism at PS/PMMA Interfacial Crack Tip:

Bimaterial interfaces are susceptible to both debonding and sliding. Mode mixity is one of its inherent features. The ratio between the stress intensity factors K_I (mode I) and K_{II} (mode II), i.e. the phase angle of a complex K , plays a significant role in interface fracture^[14]. Since PS and PMMA have approximately the same glass transition temperature and their Young's modulus and Poisson ratio are very close, the residual

stresses from the bonding process are minimal. This also leads to a very small bimaterial constant and Dundurs parameters:

$$\text{bimaterial constant: } \varepsilon = \frac{1}{2\pi} \ln \left\{ \frac{k_1 / u_1 + 1 / u_2}{k_2 / u_2 + 1 / u_1} \right\} = 0.00046 \quad (11)$$

Dundurs parameters:

$$\alpha = \frac{\Gamma(k_2 + 1) - (k_1 + 1)}{\Gamma(k_2 + 1) + (k_1 + 1)} = -0.042 \quad (12)$$

$$\text{and } \beta = \frac{\Gamma(k_2 - 1) - (k_1 - 1)}{\Gamma(k_2 + 1) + (k_1 + 1)} = -0.0014 \quad (13)$$

where u is the shear modulus; ν the Poisson's ratio, $k = 3 - 4\nu$ for plane strain, $k = (3 - 4\nu)/(1 + \nu)$ and $\Gamma = u_1 / u_2$. The subscripts 1 and 2 refer to material 1 and material 2, respectively. Therefore, from the elasticity point of view, one would expect that this PS/PMMA system would behave like a homogeneous and isotropic material. However, tests show that the pair fails with strong bimaterial characteristics. This is because PS and PMMA have quite different fracture mechanisms. Figure 7 shows the fracture surface from mode I fracture of the homopolymers. It is obvious that PMMA has a cleavage type of failure mode, whereas PS has some tearing features. Thus PMMA appears relatively brittle, whereas PS somewhat ductile.

When PS and PMMA are joined together, there are some unique characteristics at the interface crack tip, as can be seen in the picture depicted Fig.8. On the PMMA side, many microcracks emit from the interface at an oblique angle ahead of the crack tip, whereas on

the PS side a large amount of crazes oblique to the interface are found in the vicinity of interface. Fracture by crazing consumes much more energy than by microcracking. Thus, if the positive phase angle is defined such that the crack is driven into the PMMA side as shown in Fig.9, the interface would appear much weaker than if the crack is driven into the PS side for which the phase angle is negative as shown in Fig.10. It is noted that the mode mixity effect is intrinsically asymmetric. Typical fracture surfaces of a PS/PMMA interface are displayed in Fig.12. During crack propagation, PS is torn off and remains on the PMMA side, which creates many parallel lines. These lines are perpendicular to the direction of crack propagation.

From the above observation, it is clear that there exists a region at the crack tip where some nonlinear phenomena dominate. However, the load-displacement curve recorded for these PS/PMMA bimaterial specimen is linear up to the point of fracture. This indicates that nonlinear effects are confined to the region very close to the crack tip and its effects on the overall fracture behavior are negligible. Thus, one may reasonably assume that the linear elastic fracture mechanics approach is still valid to interpret the experimental data. Test results show that under a nearly mode I loading, the fracture toughness of a 200Å “thick” interface is 304 (J/m²) whereas that of a 900Å “thick” interface is 540 (J/m²). Based on this, one may draw the conclusion that thicker interface results in stronger adhesion. At the same time, one should note that a thicker interface also gives rise to stronger effect of mode mixity.

7. PS/PMMA Interfacial Crack Tip Field:

The deformation field within a small region around the crack tip was mapped by the SIEM technique. A speckle pattern, as shown in Fig.11, was created by vacuum vapor deposition. The speckle patterns before and after loading were digitally recorded and compared through an algorithm described elsewhere^[11]. Full field displacement components were calculated. Fig.13 shows such a distribution at the crack tip with the phase angle being about 17° . The measured area was about 0.5 mm by 0.4 mm. U and V represent the displacements in the horizontal and vertical directions, respectively. From these displacement fields strain distributions were computed, and the results are shown in Fig.14. The magnitudes of tangential and normal strains are of the same order of magnitude due to the large influence of mode mixity at this particular phase angle. Both shear and normal strains are seen to be concentrated within a small region. This indicates that fracture occurs under small-scale yielding conditions.

Crack opening profile and crack tip singularity were also obtained from the displacement field. The normal crack tip opening displacement (NCOD) and tangential crack tip opening displacement (TCOD) were plotted and depicted in Fig.15. It is noticed that a weak singularity exists close to the crack tip. This may be explained by the fact that

many crazes and microcracks exist at crack tip. From the crack tip opening displacement, mode mixity can be calculated. The phase angle is defined as

$$\hat{\psi} = \tan^{-1} \left(\frac{\sigma_{xy}}{\sigma_{yy}} \right)_{r=\hat{L}} \quad (14)$$

Another way to evaluate mode mixity is the ratio of normal crack opening displacement (NCOD) and tangential crack opening displacement (TCOD) as measured at a characteristic distance r which must lie within the K-annulus. Define ϕ as

$$(\tan \phi)_r = \frac{TCOD}{NCOD} \quad (15)$$

and it is related to $\hat{\psi}$ as follows:

$$(\phi)_r = \hat{\psi} + \varepsilon \ln \left(\frac{r}{\hat{L}} \right) - \tan(2\varepsilon) \quad (16)$$

8. Reference:

- [1] D. Gersappe, D. Irvine, A. C. Balazs, Y. Liu, J. Sokolov, M. Rafailovich, S. Schwarz, and D. G. Peiffer, *Science*, Vol. 265, 19 August, pp.1072-1074, 1994
- [2] T. P. Russell, A. Menelle, W. A. Hamilton, G. S. Smith, S. K. Satija and C. F. Majkrzak, *Macromolecules*, Vol.24, pp5721-5726 (1991)
- [3] L. Guo, D. Peiffer, A. Eisenberg, D. Ngyen, S. Schwarz, M. Rafailovich, J. Sokolov, "Effects of PS-PVP Random Copolymers on Adhesion of PS and PMMA --A Reactive Interface", submitted to *Maromolecules*.

- [4] H. R. Brown, K. Char and V. R. Deline, *Macromolecules*, 26, pp4155-4163 (1993)
- [5] H. R. Brown, K. Char and V. R. Deline, *Macromolecules*, 26, pp4164-4171 (1993)
- [6] C. Creton, E. J. Kramer, C. Y. Hui, and H. R. Brown, *Macromolecules*, 25, pp3075-3088 (1992)
- [7] H. R. Brown, *Journal of Materials*, 25, pp2791-2794 (1990)
- [8] M. F. Kanninen, *International Journal of Fracture*, 9, pp83-92 (1973)
- [9] N. P. O'Dowd, C. F. Shih and M. G. Stout, *Int. J. Solids Structures*, Vol.29, No.5, pp571-589, (1992)
- [10] Q. Wang and F. P. Chiang, *Composite Engineering*, 27B, pp123-128, (1996).
- [11] F. P. Chiang, Q. Wang and F. Lehman, *Nontraditional Methods of Sensing Stress, Strain and Damage in Materials and Structures*, ASTM STP 1318, Jack E. Par, Michael B. Mayor and Donald E. Marlowe, Eds., 1996 .
- [12] Q. Wang, F. P. Chiang, L. Guo, M. Rafailovich and J. Sokolov, *Fracture - Instability Dynamics, Scaling and Ductile/Brittle Behavior*, MRS Proceedings, Vol. 409, 1995
- [13] Q. Wang, S. Wu and F. P. Chiang, L. Guo, M. Rafailovich and J. Sokolov , *14th U.S. Army Solid Mechanics Symposium*, Myrtle Beach, SC. October 16-18, 1996
- [14] J. W. Hutchinson and Z. Suo, *Advances in Applied Mechanics*, 29, pp63-191 (1992)

9. Publications/Presentations Resulting From This Support:

- Q. Wang, F. P. Chiang, L. Guo, M. Rafailovich and J. Sokolov, "Micromechanical Behavior of Polymer Interface Reinforced with Copolymers", *Fracture - Instability Dynamics, Scaling and Ductile/Brittle Behavior, MRS Proceedings*, Vol. 409, 1995
- Q. Wang and F. P. Chiang, "Micromechanics Study of Fracture of Polymer Interface", *SEM's Spring Conference*, Nashville, Tennessee, 1996.
- Q. Wang, S. Wu and F. P. Chiang, L. Guo, M. Rafailovich and J. Sokolov, "Polymer Interface Reinforced with Copolymers - An Experimental Micromechanics Study", *14th Army Solid Mechanics Symposium*, Myrtle Beach, South Carolina, October 16-18, 1996
- Q. Wang and F. P. Chiang, "Fracture Behavior of PS/PMMA Interface Reinforced with Block Copolymer", 1998 US National Congress of Applied Mechanics, Florida.

10. Personnel Participated in This Project

F. P. Chiang: Principal Investigator

M. Rafailovich: Professor of Material Science and Engineering

J. Sokolov: Associate Professor of Material Science and Engineering

Q. Wang: graduate student, Department of Mechanical Engineering

S. Wu and L. Guo: graduate students, Department of Material Science and Engineering

A-B copolymer

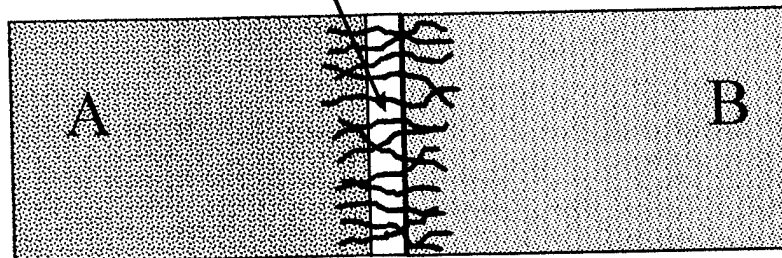


Figure 1. A-B block copolymer reinforced interphase between A and B homopolymers.

PMMA backbone: (MW)120 K

PS chains: (MW) 3x40 (K)

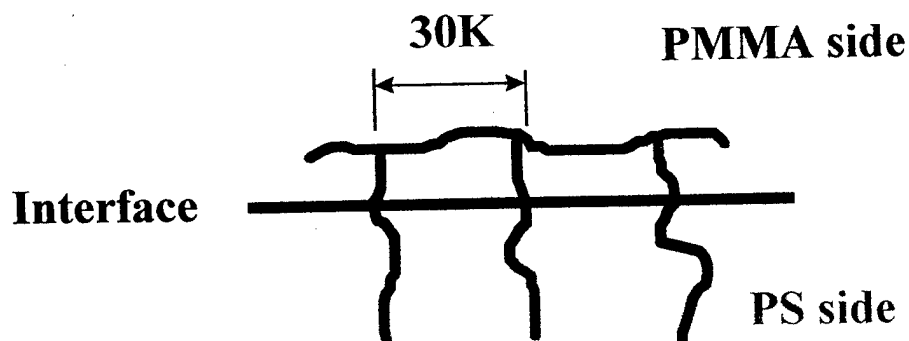


Figure 2. Architecture of PS-g-PMMA graft copolymer.

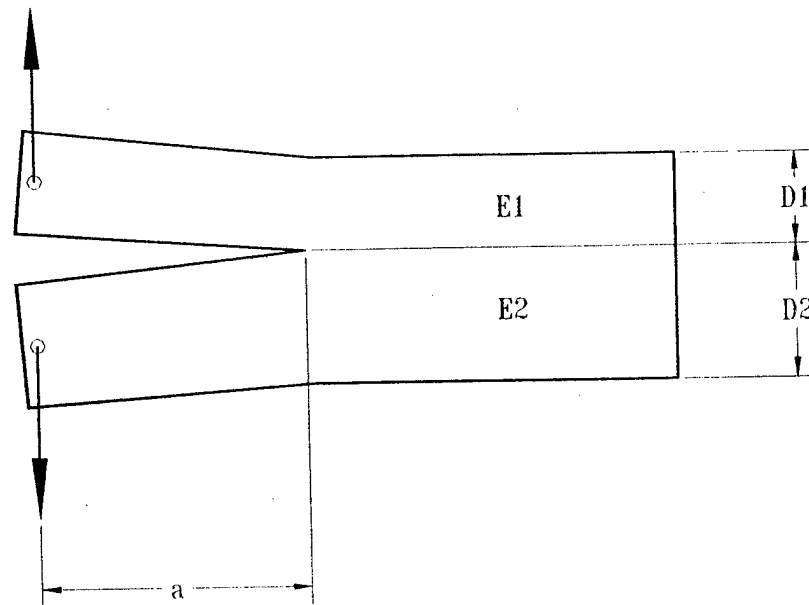


Figure 3. Asymmetric double cantilever beam test

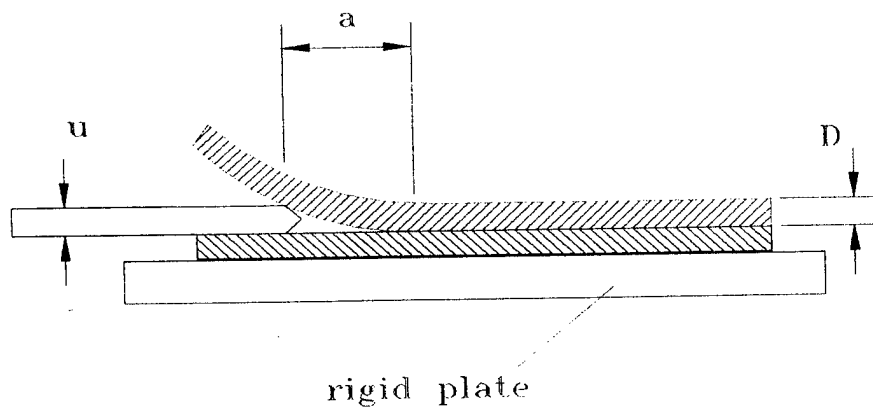


Figure 4. Wedge open interfacial crack between a single cantilever beam and a elastic foundation

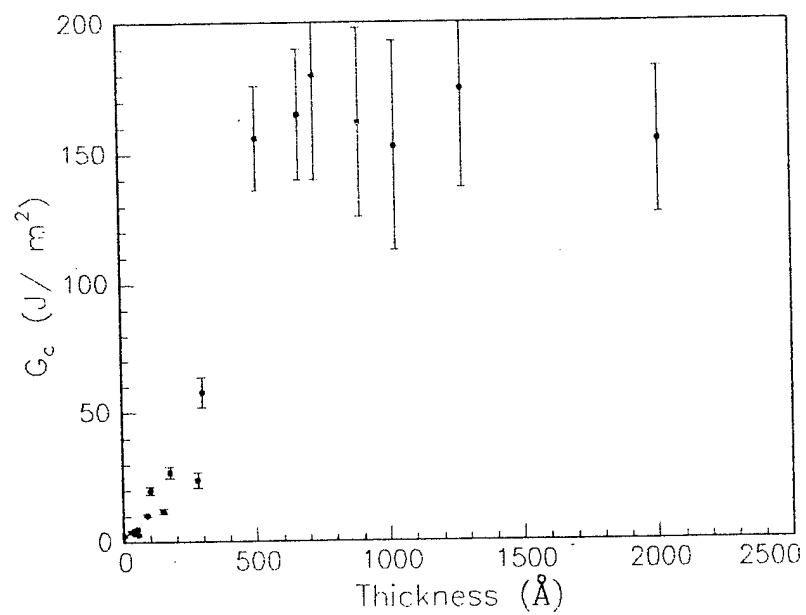


Figure 5. Fracture toughness G_c increases with the “thickness” of copolymer interphase.

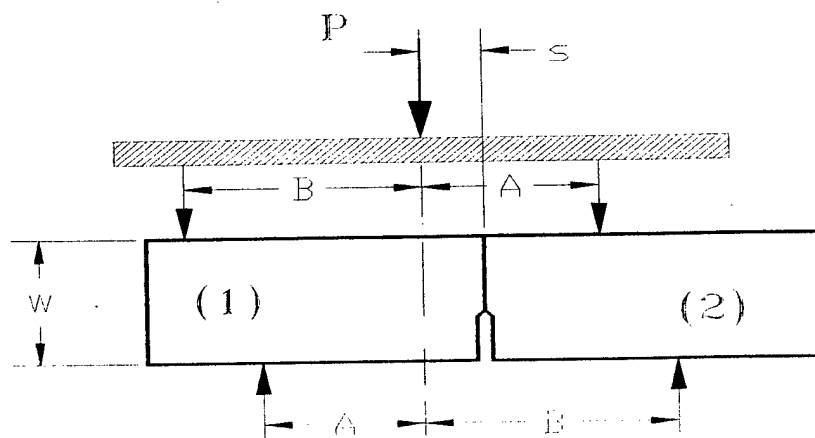


Figure 6. Asymmetric four point bend test.

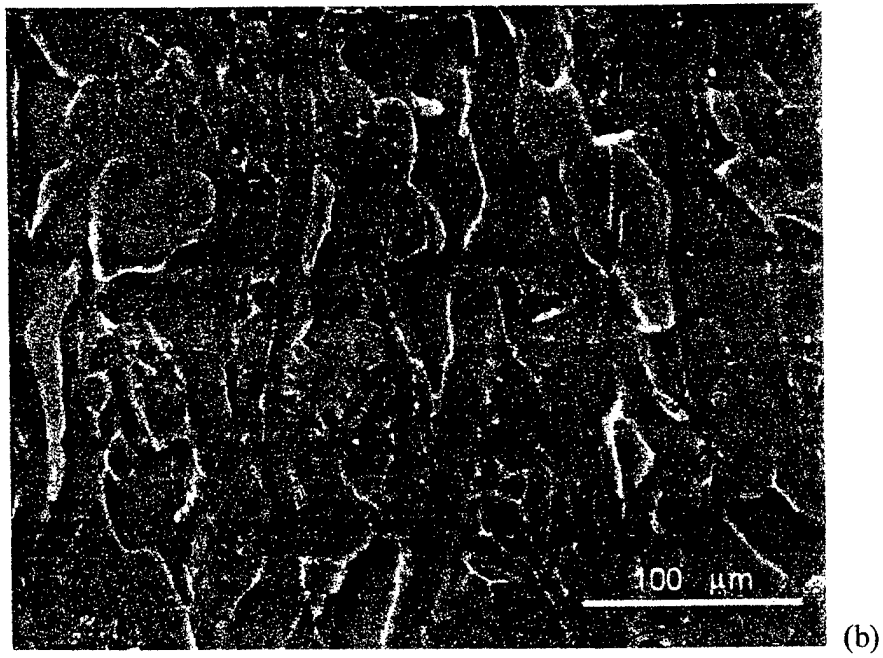
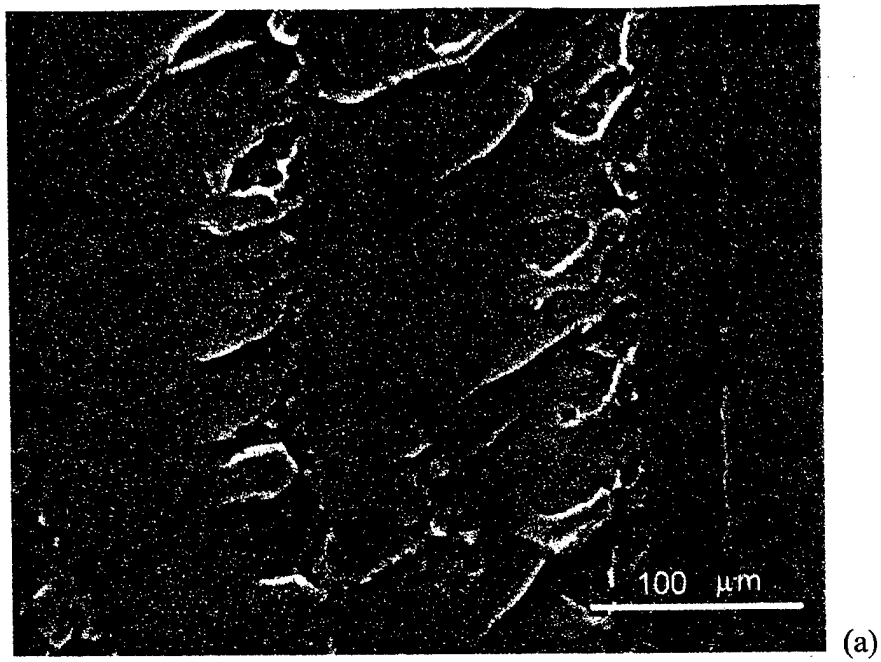


Figure 7. Fracture surface of (a) PMMA and (b) PS specimens

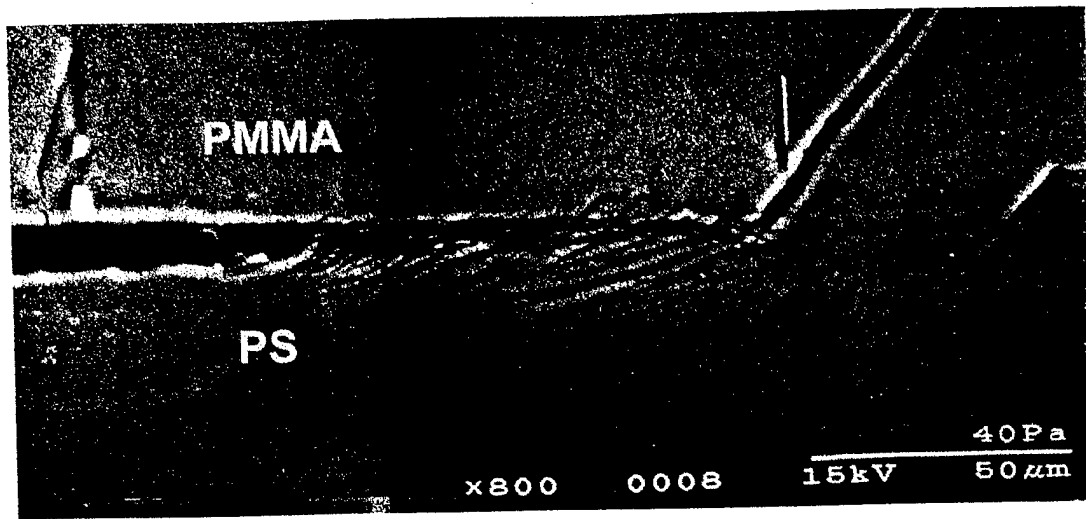


Figure 8. Features near the tip of PS/PMMA interfacial crack.

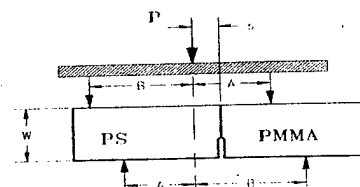
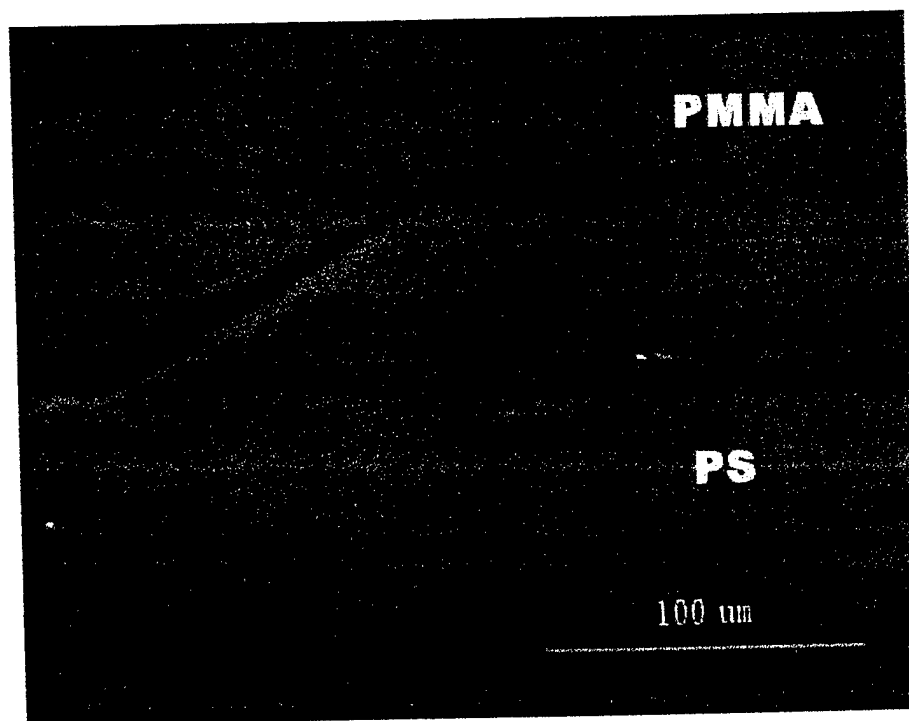


Figure 9. Failure mechanism under positive phase angle.

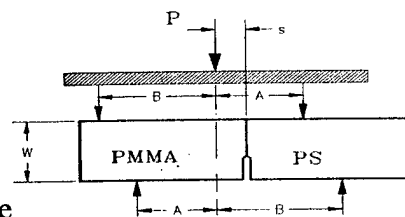
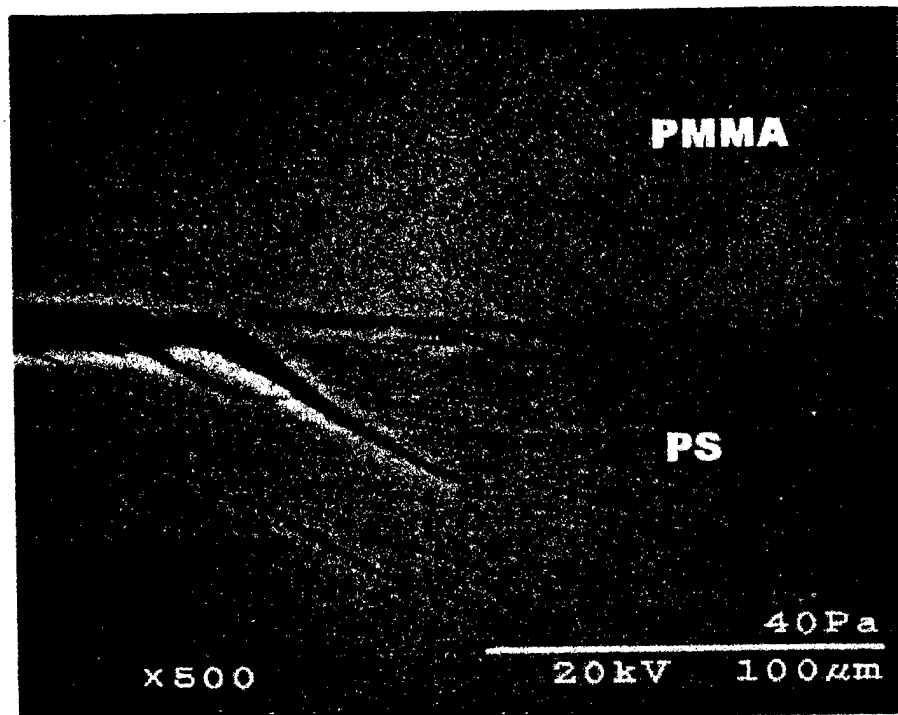


Figure 10. Failure mechanism under negative phase angle

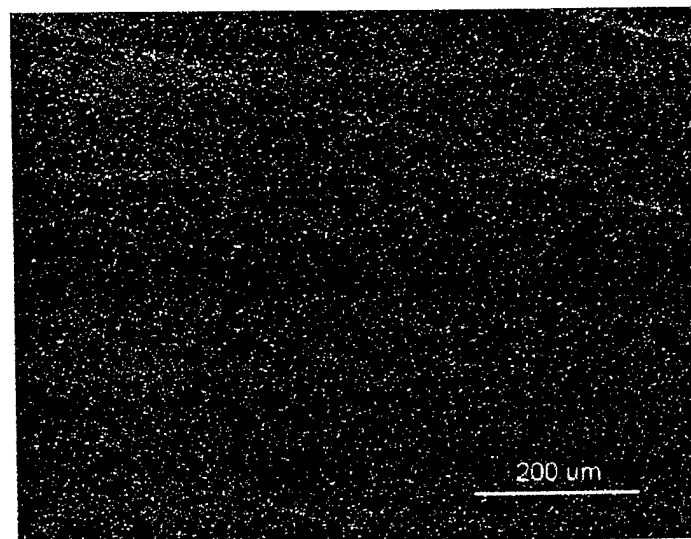


Figure 11. A typical speckle pattern created from vacuum deposition.

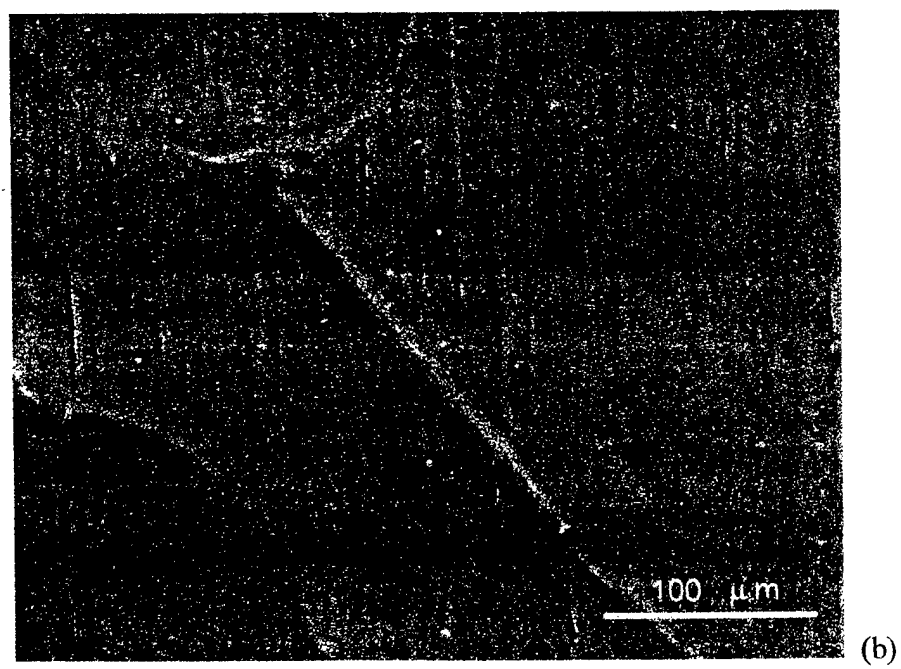
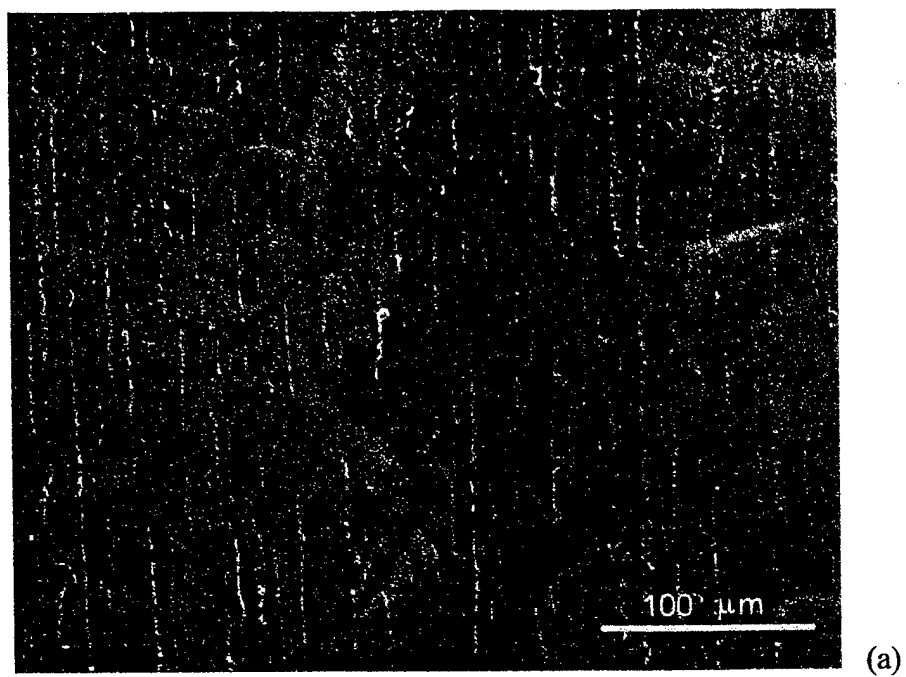


Figure 12. Fracture surface of bimaterial interface on (a) PMMA and (b) PS sides.

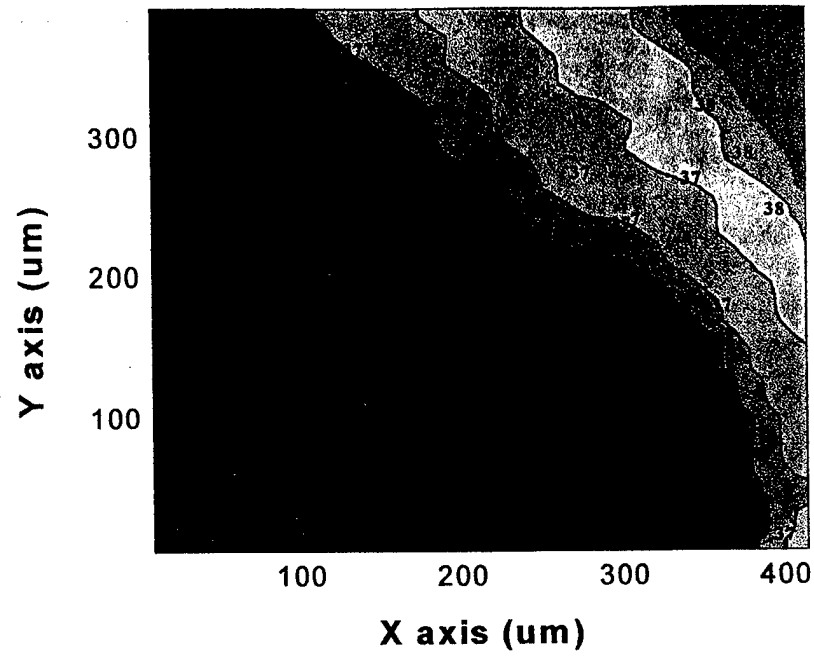


Figure 13(a) U-displacement contour

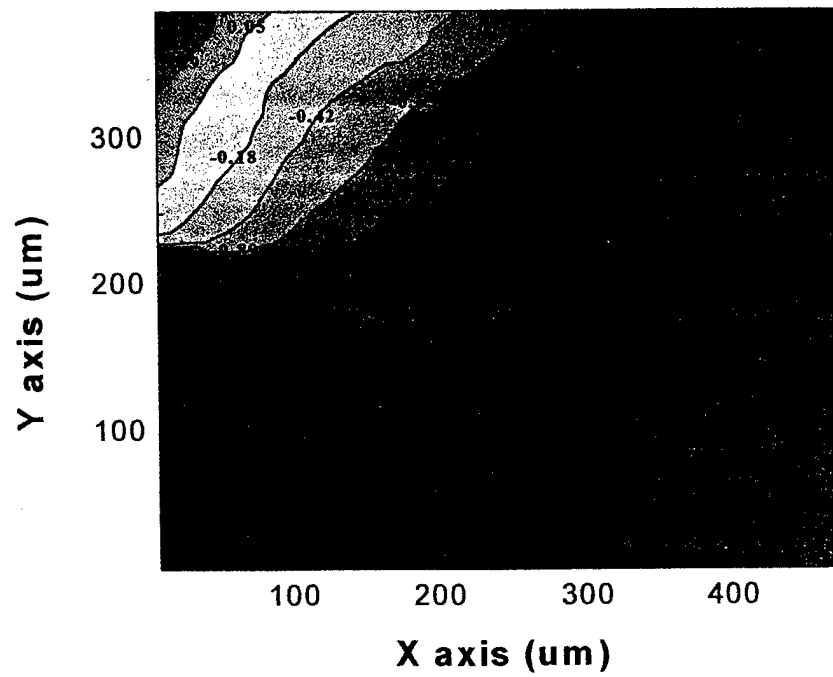


Figure 13(b) V-displacement contour

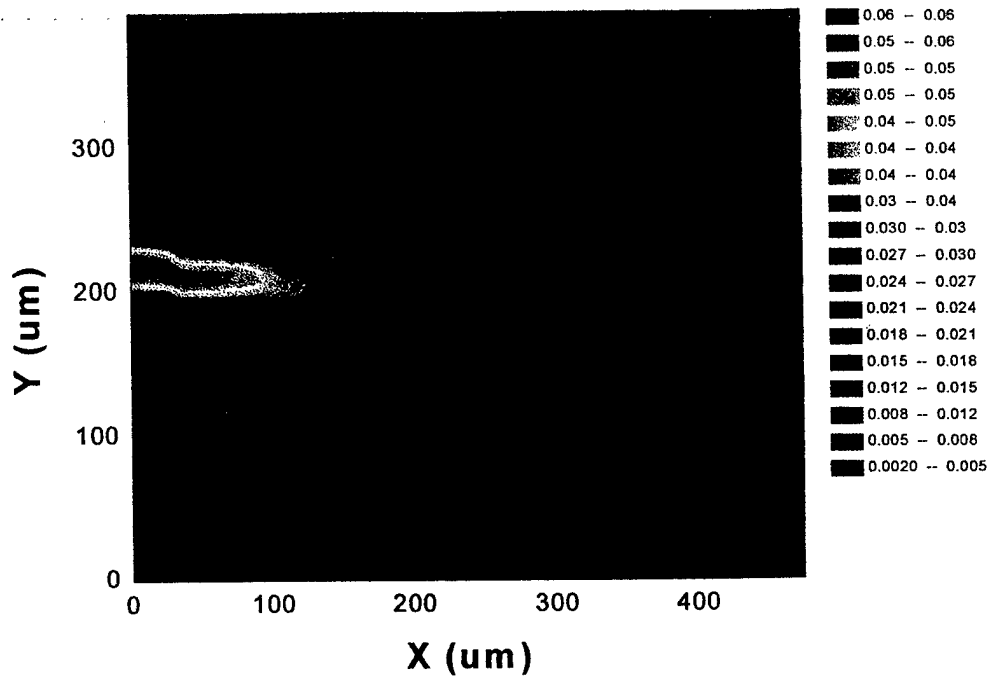


Figure 14(a) Distribution of normal strain ϵ_{yy}

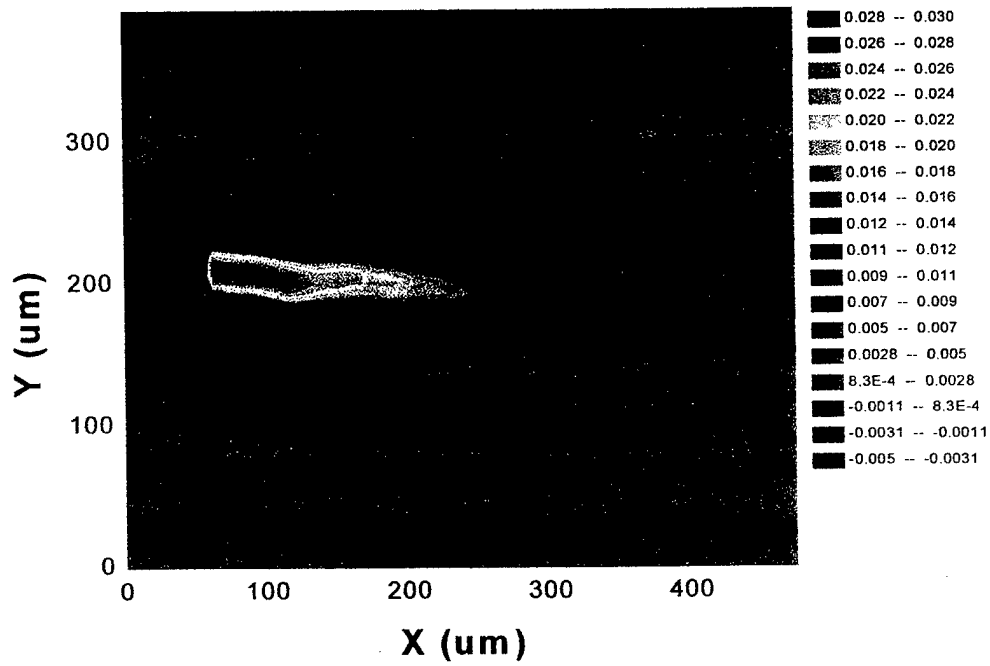


Figure 14(b) Distribution of normal strain ϵ_{xy}

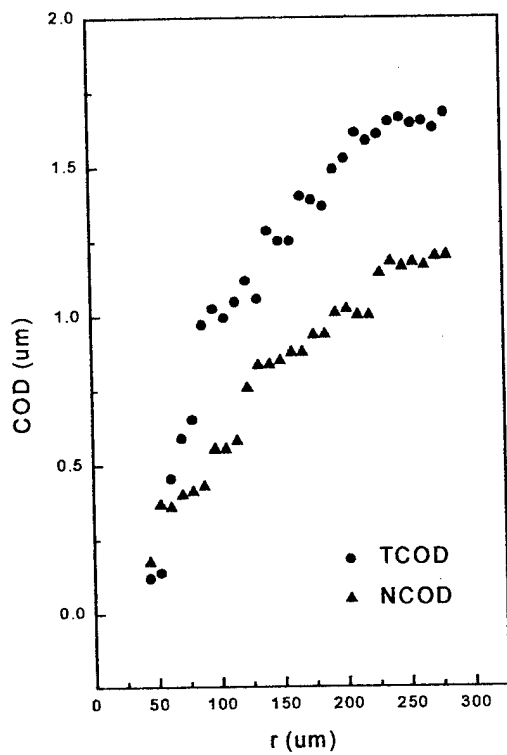


Figure 15(a)
Crack tip opening displacement

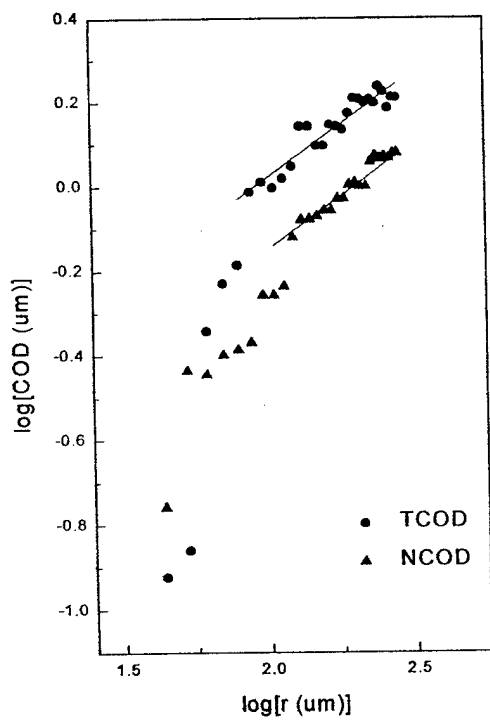


Figure 15(b)
Crack tip singularity